Applied Physics A (2020) 126:294
https://doi.org/10.1007/s00339-020-03472-y

Applied Physics A
Materials Science & Processing

Preparation of tetragonal barium titanate nanopowders by microwave solid-state synthesis

Haoyu Qian[1] · Guisheng Zhu[1] · Huarui Xu[1] · Xiuyun Zhang[1] · Yunyun Zhao[1] · Dongliang Yan[1] · Xianyong Hong[1] · Yin Han[1] · Zhenxiao Fu[1] · Shiwo Ta[2] · Aibing Yu[3]

Received: 18 December 2019 / Accepted: 16 March 2020 / Published online: 26 March 2020

Abstract
Tetragonal-phase $BaTiO_3$ powders of particle size 370 nm were synthesized by microwave sintering at 850 °C. The raw materials were $BaCO_3$, TiO_2, and alanine. SiC microspheres were used as microwave conductors. The effects of the holding time, sintering aids, and SiC addition on the preparation of $BaTiO_3$ were investigated. The results indicate that the addition of SiC as a microwave acceptor leads to formation of microwave micro-regions. This enables uniform heating of the raw materials and decreases the calcination temperature needed to obtain $BaTiO_3$. Alanine coordinates with Ba, and this loosens the metal–CO_3 bond and promotes separation of CO_2, decreases the $BaCO_3$ decomposition temperature, and provides a higher nucleation site density. It gives an idea about the microwave solid-state synthesis of $BaTiO_3$ powder.

Keywords $BaTiO_3$ · Tetragonal · SiC · Alanine · Microwave micro-region sintering

1 Introduction

Perovskite oxide has many properties, e.g., piezoelectric, dielectric, and ferroelectric activities [1,2]. $BaTiO_3$ is an important perovskite structure material. It is used in multilayer ceramic capacitors (MLCCs), semiconductors, and electroluminescent panels [3,4]. The trend toward miniaturization of components in the electronics industry has increased interest in perovskite oxide nanopowders. For example, the fabrication of high-capacitance, small MLCCs requires the solid-state production of tetragonal-phase $BaTiO_3$ nanopowders with small highly dispersed particles [5]. The development of methods for decreasing the particle size and improving the uniformity of the $BaTiO_3$, while decreasing the synthesis temperature, is therefore a key issue.

$BaTiO_3$ can be synthesized by sol–gel [6,7], solid-state [8,9], hydrothermal [10,11], coprecipitation [12], and microwave methods [13]. $BaTiO_3$ prepared by liquid-phase methods has hydroxyl lattice defects, and this leads to MLCC porosity during sintering [14]. $BaTiO_3$ has been synthesized by a solid-state method below 1000 °C, with $BaCO_3$ and TiO_2 as the raw materials [15]. Although solid-state methods are cheap and simple, the products have a large average particle size, high agglomeration, and poor chemical homogeneity, and are not suitable for use in miniaturized electronic devices [16]. However, $BaTiO_3$ powder synthesized by a solid-state method is crystalline and has fewer surface defects than $BaTiO_3$ prepared by liquid-phase methods. It has good dielectric properties, and its use ensures reliability of MLCCs. Companies such as Taiyo Yuden in Japan are therefore still developing improved solid-state methods for preparing tetragonal $BaTiO_3$ with small particles. Ando et al. [17] tried to solve the problems associated with solid-state reactions by adding bovine serum albumin to decrease the decomposition temperature of $BaCO_3$ in the presence of TiO_2; this decreases the calcination temperature in $BaTiO_3$ synthesis. Rui et al. [18] synthesized $BaTiO_3$ via energy ball milling, which decreased the particle size,

✉ Guisheng Zhu
zhuguisheng@guet.edu.cn

[1] Guangxi Key Laboratory of Information Materials, Engineering Research Center of Electronic Information Materials and Devices, Ministry of Education, Guilin University of Electronic Science and Technology, Guilin 541004, China

[2] State Key Laboratory of Advanced Materials and Electronic Components, Guangdong Fenghua Advanced Technology Holding Co., Ltd, Zhaoqing 526020, China

[3] Department of Chemical Engineering, Monash University, Clayton, VIC 3800, Australia

increased the uniformity of the raw materials, and decreased the reaction temperature. Microwave solid-state synthesis is a new method that has emerged in recent years. Gromov et al. [19] placed a high-purity graphite pellet under a crucible as a secondary acceptor to absorb microwave radiation, which decreased the calcination temperature, to obtain $BaTiO_3$ powders. Rataro et al. [20] used ultrasonication and microwave irradiation, respectively, instead of classical ball mixing and synthesis steps, to obtain $BaTiO_3$. The synthesis of highly dispersed $BaTiO_3$ nanopowders is therefore a challenge.

In this work, we used a combination of a solid-state method and microwave irradiation to prepare tetragonal $BaTiO_3$ from $BaCO_3$, TiO_2, and alanine as the raw materials. Alanine has C=O and >NH groups, which coordinate preferentially with the ligand field of Ba. This lowers the $BaCO_3$ decomposition temperature and decreases the calcination temperature. Because $BaCO_3$ and TiO_2 are weak microwave acceptors, a secondary acceptor, namely SiC, was added. This additive must efficiently absorb microwave radiation, be chemically inert, decrease the synthesis temperature, and be readily separable after completion of the process. Unlike traditional solid-state methods, this method enables calcination below 900 °C and provides tetragonal $BaTiO_3$. The product has promising applications in miniaturization of electronic devices.

2 Experimental

2.1 Sample fabrication

A $BaTiO_3$ nanopowder was synthesized from commercially available $BaCO_3$ (99.99%, Guangdong Fenghua Advanced Technology (HOLDING) Co., Ltd., Zhaoqin, China) and TiO_2 (99.99%, Guangxi Jinmao Titanium Industry Co., Ltd., Wuzhou, China). A mixture of $BaCO_3$ and TiO_2 in water was ground by sand milling with 0.3 mm ZrO_2 balls (BYZR-03, Shenzhen Chemical Boyi Industrial Co., Ltd., Shenzhen, China) at 2200 rpm for 6 h. The mixture was dried at 80 °C for 12 h. Then, 5 wt% alanine (99.99%, Shanghai Aladdin Bio-Chem Technology Co., Ltd., Shanghai, China) was added to $BaCO_3$ and TiO_2 in water under ball milling, and dried by spraying. SiC gravel (99.99%, Meiqilin New Materials Co., Ltd., Wuhan, China) was mixed with the spray-dried materials by mechanical stirring, and the mixture was transferred to a microwave furnace (HY-QS3016, Hunan Huaye Microwave Technology Co., Ltd., Hunan, China). The frequency was set at 2.45 GHz, and the mixture was heated to 850 °C at a rate of 30 °C/min and then held for 2 h. The temperature was measured with an infrared instrument. Figure 1 shows a schematic diagram of the interior of the microwave oven. The SiC was separated mechanically.

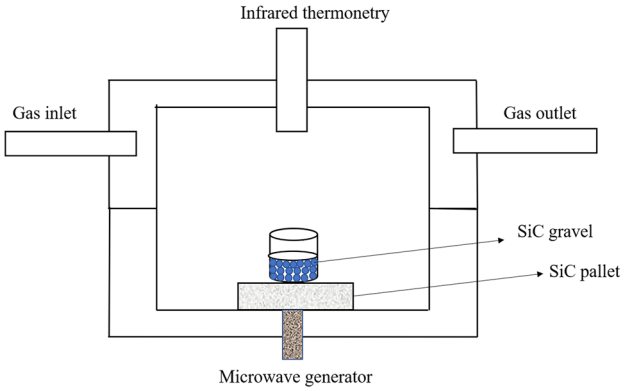

Fig. 1 Schematic diagram of interior of microwave oven

Figure 2 shows a flow chart of the microwave synthesis of the $BaTiO_3$ powder.

2.2 Characterization

The crystal phases of the $BaTiO_3$ samples were investigated by X-ray diffraction (XRD; D8 Advance, Germany) with Cu Kα radiation and a step size of 0.02°/s in the 2θ range 20°–70°. Changes in the electronic states caused by alanine addition and milling were evaluated by X-ray photoelectron spectroscopy (XPS; Thermo ESCALAB250). Mass losses of the raw materials were investigated by thermogravimetry (TG). The sample microstructures were examined by field-emission scanning electron microscopy (FE-SEM; FEI Tecnai-450, USA). The $BaTiO_3$ structure was examined by Raman spectroscopy (Rwlishes, France) and Fourier transform infrared (FTIR) spectroscopy (Nicolet 6800, The Netherlands). Impurity elements in $BaTiO_3$ were identified by inductively coupled plasma atomic emission spectroscopy (ICP-AES; Varian, UK). The particle size distribution of the $BaTiO_3$ powder was determined with a Mastersizer 2000 (UK).

3 Results and discussion

3.1 Effects on $BaTiO_3$ microstructure of different holding times during microwave synthesis

The effects on $BaTiO_3$ of the weight percentage of SiC and holding time were investigated by synthesizing two groups of samples, group A and B, under different conditions; details are shown in Table 1. Figure 3 shows XRD and spectroscopic data for $BaTiO_3$ nanopowders (group A) prepared by microwave solid-state sintering with different holding times. As the holding time increased from 0.5 to 4 h, the structure changed from cubic to tetragonal and the

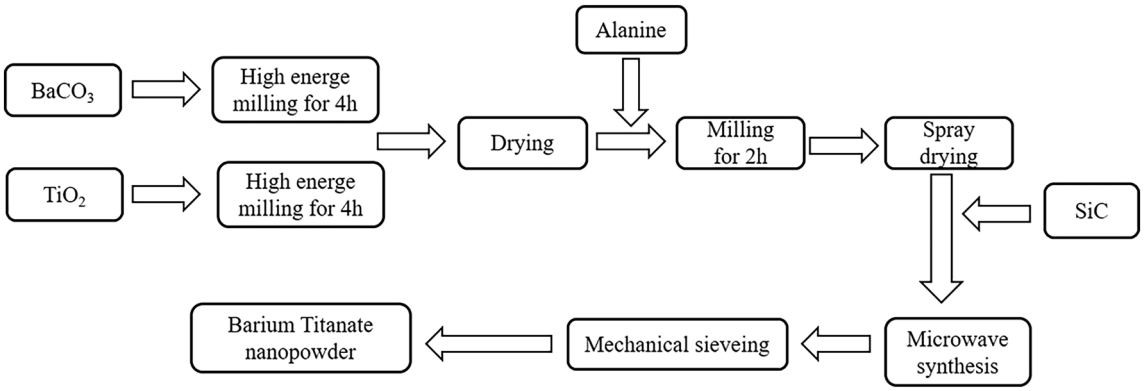

Fig. 2 Flow chart of microwave synthesis of $BaTiO_3$ powder

Table 1 $BaTiO_3$ samples synthesized by microwave solid-state method, and lattice parameters determined by XRD

Sample	Calcination temperature (°C)	Hold time (h)	The ratio of Sic gravel (wt%)	Lattice parameters	Tetragonality (*c*/*a*)
A					
S1	850	0.5	20	a = 4.0017, c = 4.0029	1.0002
S2	850	1	20	a = 3.9918, c = 4.0229	1.0078
S3	850	2	20	a = 3.9947, c = 4.0285	1.0085
S4	850	4	20	a = 3.9913, c = 4.0284	1.0093
B					
S5	850	2	0	a = 3.9928, c = 3.9940	1.0001
S6	850	2	10	a = 4.0012, c = 4.0263	1.0063
S7	850	2	20	a = 3.9947, c = 4.0285	1.0085
S8	850	2	25	a = 3.9922, c = 4.0285	1.0091

XRD peak intensities increased, as shown in Fig. 3a. For the samples prepared with holding times of 0.5 and 1 h, $BaCO_3$ was detected and the patterns of the prepared $BaTiO_3$ samples correspond to JCPDS card (31-0174). When the holding time was increased, the $BaCO_3$ peak disappeared. The samples prepared with holding times of 2 and 4 h, i.e., S3 and S4, respectively, correspond to pure tetragonal $BaTiO_3$ (PDF 75–0460). The $BaTiO_3$ phases, i.e., cubic and tetragonal, are generally distinguished by the absence or presence in the XRD pattern of a double diffraction peak near $2\theta \approx 45°$ [21]. Figure 3a shows that when the holding time was increased, the diffraction peak at $2\theta \approx 45°$ eventually split into two peaks and became more apparent; these peaks correspond to the (200) and (002) planes of tetragonal-phase $BaTiO_3$ [22]. This is because with increasing holding time, $BaTiO_3$ undergoes a crystal-phase transformation. The lattice parameter a decreases and c increases, as shown in Table 1. Low-tetragonal cubic-phase $BaTiO_3$ was obtained by composite-hydroxide-mediated synthesis, and tetragonal-phase $BaTiO_3$ was obtained by solid-state synthesis. This suggests that the addition of SiC enabled uniform microwave sintering, which enables shortening of the holding time and promotes the phase transition to tetragonal. The tetragonality values of the group A samples (determined from the *c*/*a* ratio) are 1.0002, 1.0078, 1.0085, and 1.0093 for S1, S2, S3, and S4, respectively [23,24]. The content of the tetragonal phase was calculated by using the following formula [25]:

$$\mathrm{d}\left(\frac{\mathrm{c}}{\mathrm{a}}\right) = d\left(\frac{\sin\theta 2}{\sin\theta 1}\right) \approx \frac{\cos\theta 1}{2\sin\theta 2} d(\Delta 2\theta) \approx 1.2 * d(\Delta 2\theta) \quad (1)$$

where $\theta 1$ and $\theta 2$ correspond to the (002) and (200) planes, respectively. Quantitative analysis of S1, S2, S3, and S4 by using the MDI Jade 5.0 software showed that the tetragonal-phase content increased from 18.2 (S1) to 97.3% (S4). The presence of $BaCO_3$ in the samples was detected by FTIR spectroscopy; the spectra of $BaTiO_3$ samples S1–S4 are shown in Fig. 3b. The spectra of S1 and S2 have two weak absorption peaks at 1439.11 and 858.69 cm^{-1}; these verify the presence of $BaCO_3$ [26]. The $BaCO_3$ peaks gradually disappeared with increasing holding time. The FTIR spectra confirm the results obtained by XRD. Tetragonal-phase $BaTiO_3$ can be obtained by increasing the holding time.

Figure 3c shows the Raman spectra of the $BaTiO_3$ samples prepared with different holding times. The figure shows

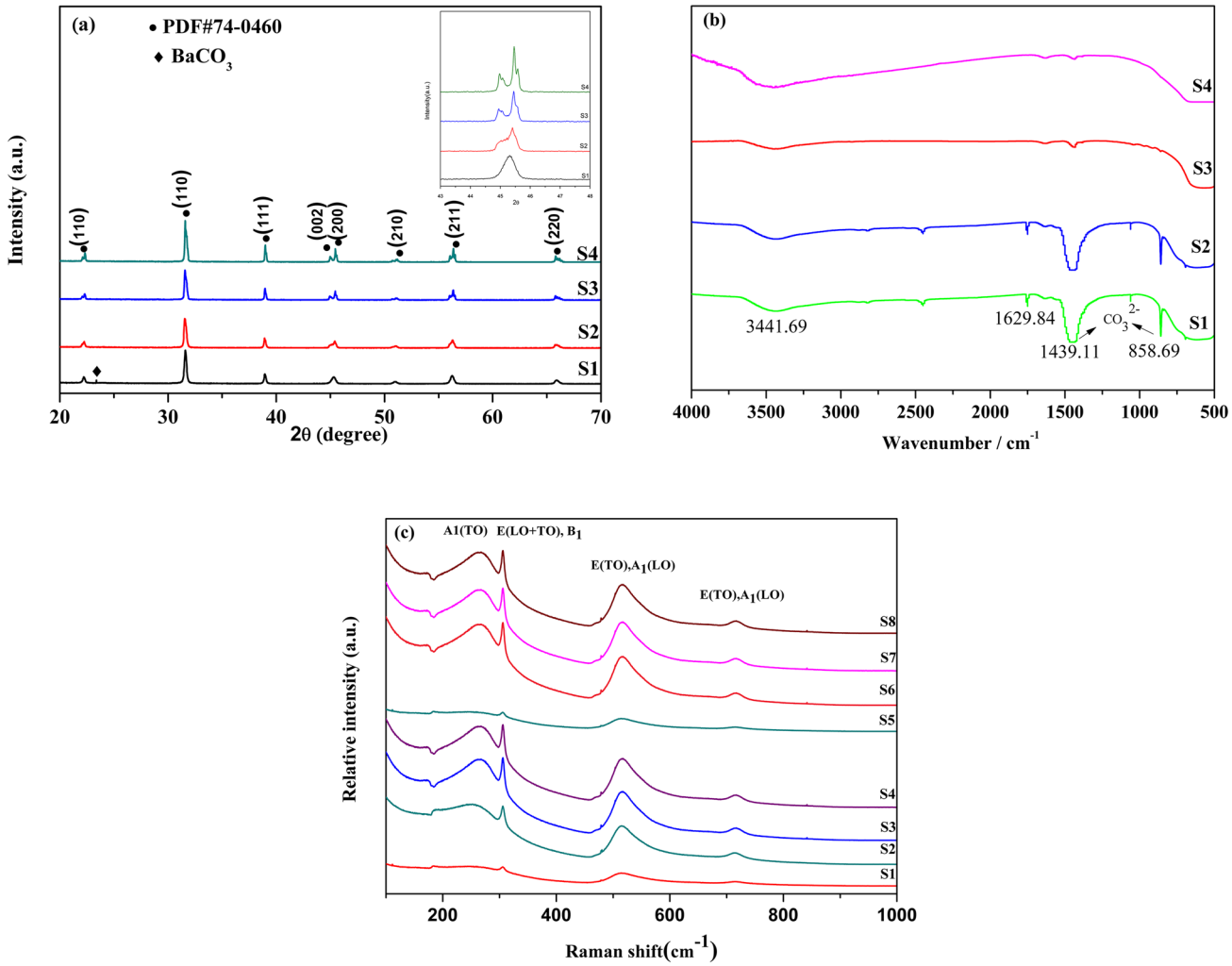

Fig. 3 XRD and spectroscopic data for $BaTiO_3$ prepared by microwave solid-state method with different holding times

that the spectrum of the sample synthesized at 850 °C for 0.5 h contains no obvious peak from the $BaTiO_3$ tetragonal phase, which indicates that it has no Raman activity [27]. When the cubic phase is transformed to the tetragonal phase, broad peaks appear near 260 and 520 cm^{-1}; these are attributable to changes in the Ti^{4+} position in the cubic-phase $BaTiO_3$ lattice and indicate Raman activity. The Raman peaks near 304 and 720 cm^{-1} are characteristic of tetragonal $BaTiO_3$ [28]. As the holding time increases, the intensities of the Raman peaks at 304 and 720 cm^{-1} increase, which indicates increasing tetragonality of the $BaTiO_3$ samples; this is confirmed by the XRD patterns.

Table 2 shows the particle sizes of $BaTiO_3$ samples synthesized at 850 °C with different holding times. The synthetic process involves growth of $BaTiO_3$ grains and a crystal transition from the cubic phase to the tetragonal phase. The solid-state reaction is not sufficient when the holding time is 0.5 h. When the holding time is too short, cubic-phase $BaTiO_3$ is obtained. Laser particle size analysis of sample S1 shows that grain growth is not complete and $BaCO_3$ impurities are still present in the product; this is consistent with the results shown in Fig. 3. With increasing holding time, the $BaCO_3$ impurities disappear and grain growth is complete. The particle size of the $BaTiO_3$ nanopowders increased linearly because of microwave micro-region sintering. The D_{50} values for S1, S2, S3, and S4 are 270, 300, 370, and 650 nm, respectively. The

Table 2 Statistical distributions of particle sizes

Sample	D_{10} (nm)	D_{50} (nm)	D_{90} (nm)	BET (m^2/g)
S1	150	270	400	8.56
S2	180	300	700	5.93
S3	280	370	540	7.32
S4	320	650	820	3.66

corresponding specific surface areas are 8.56, 5.93, 7.32, and 3.66 m^2/g.

3.2 Effects of alanine sintering aid on $BaTiO_3$

The solid-state reactions of TiO_2 and $BaCO_3$ can be represented by Eqs. (2) and (3) [29]:

$$BaCO_3 + TiO_2 \rightarrow BaTiO_3 + CO_2 \uparrow \quad (2)$$

$$BaTiO_3 + BaCO_3 \rightarrow Ba_2TiO_4 + CO_2 \uparrow \quad (3)$$

Figure 4a shows that the TG curves do not reflect reactions (2) and (3). The sample weight loss when alanine was added was complete at 820 °C, and the sample weight loss without alanine addition was complete at 900 °C. This confirms that the experimental method involves reaction (2) almost entirely, because reaction (3) occurs above 1000 °C [30]. The thermal decomposition behaviors of alanine and mixtures of alanine with Ti and Ba inorganic compounds are compared in Fig. 4b. Complete decomposition of alanine occurs at 227 °C, but the differential TG curves of alanine mixed with the raw materials are multimodal; 38% of the organic matter was present up to 342 °C. The weight loss curve indicates that alanine decomposition occurs in stages; the portion that coordinates with the metal ions can survive to a higher temperature. In this study, the differential TG curves for alanine with $BaCO_3$, TiO_2, and a mixture of the two, show that weight loss begins at around 200 °C because the desorbed excess alanine does not directly coordinate with the metal species [31]; the details are shown in Table 3. The data in Table 3 show that the weight loss at around 200 °C for alanine–$BaCO_3$–TiO_2 equals the difference between those for alanine–$BaCO_3$ and alanine–TiO_2. This indicates that alanine can be adsorbed on the surfaces of $BaCO_3$ and TiO_2. The rest of the alanine is then combusted at around 280 °C for alanine–TiO_2 and alanine–$BaCO_3$–TiO_2, and 332 °C for alanine–$BaCO_3$. It can be assumed that a portion of the alanine is adsorbed or coordinated on the surfaces of $BaCO_3$ and TiO_2

Table 3 Thermal decomposition behaviors of alanine and mixtures of alanine with Ba/Ti inorganics

Samples	Decomposition temperature (°C)	Weight loss (%)
Alanine	227	100
$BaCO_3$–TiO_2–Alanine	208	28
	282	72
$BaCO_3$–Alanine	205	52
	332	48
TiO_2–Alanine	185	22
	276	62
	347	16

Figure 5 shows the changes in the O1s and Ba3d binding energies after addition of alanine. Figure 5a shows that after alanine was added, the Ba3d peak shifted by 0.7 eV compared with the corresponding peak for $BaCO_3$ without added alanine. This indicates that coordination of the added alanine with Ba^{2+} resulted in a decrease in the CO_3^{2-} bond energy. The O1s peak position and energy transfer after mixing TiO_2 with alanine are not much different from those for TiO_2. Figure 5b shows that the O1s binding energy of $BaCO_3$ shifted by 0.5 eV after alanine addition [32]. These results indicate that alanine and Ba^{2+} play important roles

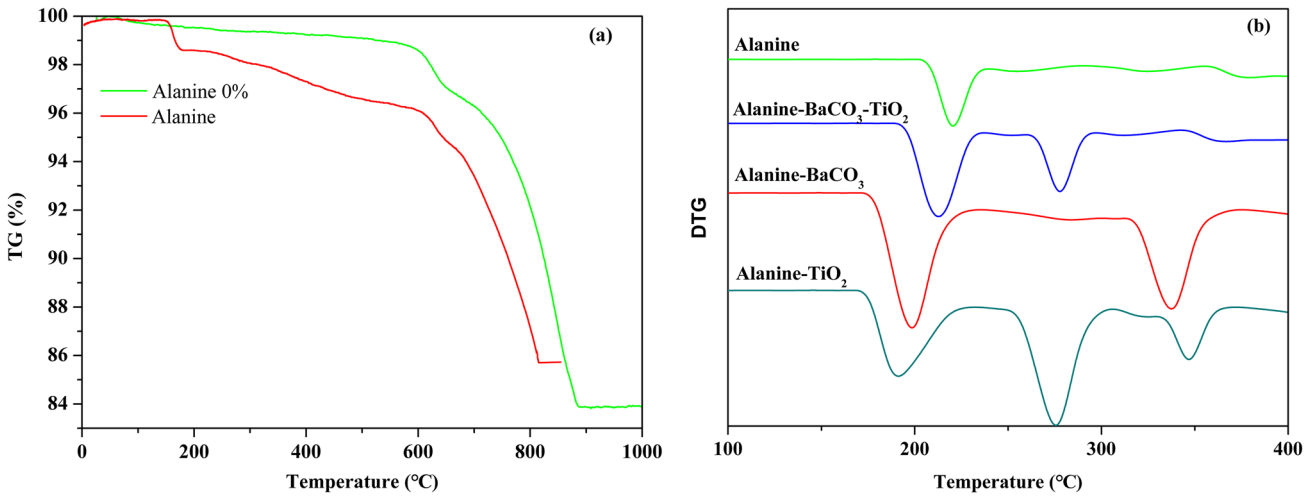

Fig. 4 Thermogravimetric analysis of samples: **a** TG profiles of samples with alanine and **b** differential TG curves of alanine mixed with Ba/Ti inorganics

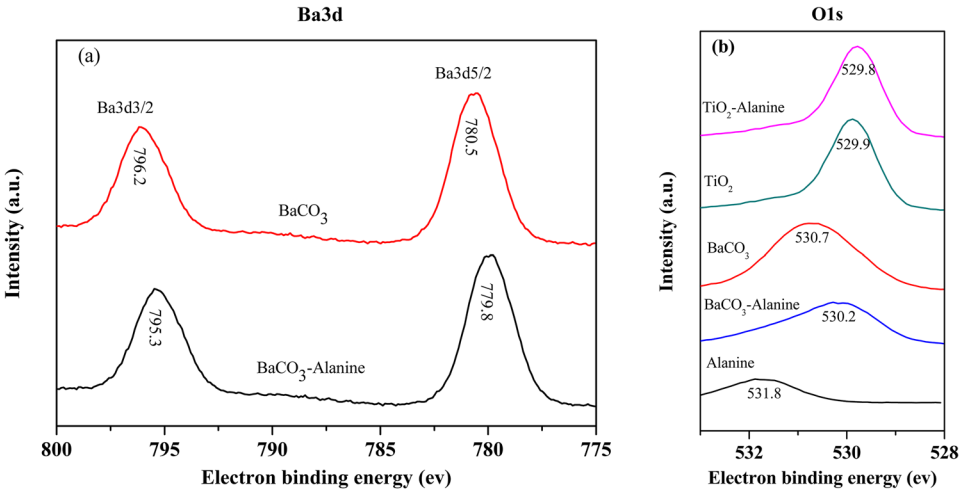

Fig. 5 XPS spectra: **a** Ba3d and **b** O1s

in the process and confirm that alanine helps to lower the temperature of $BaTiO_3$ synthesis.

3.3 Effects of SiC content on microstructures of $BaTiO_3$ powders

When a dielectric material is placed in a microwave field, it couples with the microwave field and electromagnetic energy is converted to thermal energy. $BaCO_3$ and TiO_2 are weak microwave acceptors at room temperature, which results in hysteresis in the microwave heat transfer efficiency. A secondary acceptor, i.e., SiC, was added to improve the microwave heat transfer efficiency. The dielectric loss of SiC therefore determines the efficiency of heating of the raw materials. In this study, a SiC plate was added to the underside of a corundum crucible, and SiC gravel was mixed with the powders by mechanical stirring to form a $BaCO_3$–SiC–TiO_2–alanine symbiotic system, and a uniform temperature distribution was achieved in the microwave field. This promoted formation of small, uniform particles of tetragonal-phase $BaTiO_3$. We found that without addition of SiC to the raw materials, microwave heating for 30 min to reach 900 °C and holding for 2 h gave $BaTiO_3$, but the tetragonality was poor. When SiC was added to the raw materials, thermal runaway occurred and the heating rate increased. This can be attributed to the microwave absorption capacity of SiC. The power (P) absorbed by the dielectric material is calculated by using Eq. (4).

$$P = \frac{1}{2}\sigma\left|E^2\right| + \omega\varepsilon_0\varepsilon_r''|E|^2 + \omega\mu_0\mu_r''\left|H\right|^2 \quad (4)$$

where electrical conductivity is denoted by σ, the amplitudes of the electric and magnetic fields are $|E|$ and $|H|$, respectively, the applied microwave frequency is denoted by ω, the dielectric constant and permeability of free space are denoted by ε_0 and μ_0, respectively, and ε_r'' and μ_r'' are the relative dielectric constant and the imaginary part of the permeability, respectively. $BaCO_3$ and TiO_2 have poor absorption properties. Equation (4) expresses the total energy absorbed by SiC. Consequently, $BaTiO_3$ was prepared in a short time, and the synthesis temperature was 850 °C, which is lower than the phase transition temperature (900 °C). However, the internal temperature of the sample can be higher than 850 °C because of the microwave heating mechanism. The core temperature of the raw materials cannot be directly measured because there is a distance between the sample and the infrared thermometer, and only the surface temperature can be measured. It can be assumed that the core temperature of the sample was higher than the phase transition temperature of $BaTiO_3$.

In the experiments, $BaTiO_3$ was prepared by microwave solid-state synthesis at 850 °C, but $BaCO_3$, TiO_2, and alanine are poor microwave acceptors, therefore, a secondary acceptor, namely SiC, was added. In this study, the effects on the sample properties of the amount of added SiC were investigated; the details are given in Table 1. Figure 6 shows the XRD patterns of the samples in group B, which were synthesized at 850 °C for 2 h with different SiC contents. The $BaTiO_3$ sample prepared without added SiC is cubic phase and corresponds to JCPDS card (31-0174). When the SiC content was increased, the XRD patterns show that the obtained samples (S6–S8) correspond to $BaTiO_3$ (JCPDS No. 75-0460). These results indicate that with increasing SiC content from 0 to 25 wt%, the tetragonality values of the synthesized $BaTiO_3$ (group B samples) increased from 1.0001 to 1.0091. This is in agreement with the Raman spectroscopic results.

Figure 7 shows SEM images of $BaTiO_3$ samples prepared at 850 °C for 2 h with different SiC contents. Figure 7a shows that the cubic-phase $BaTiO_3$ sample, which

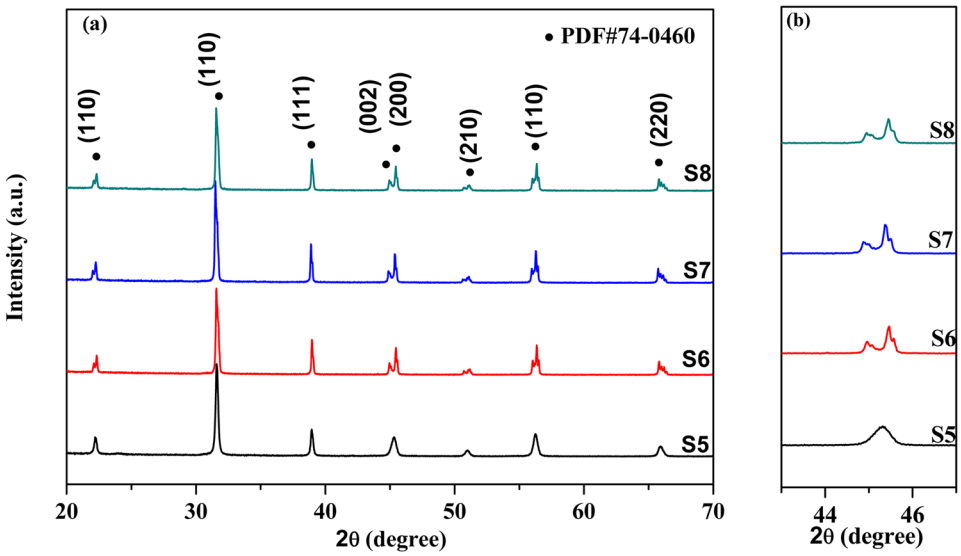

Fig. 6 XRD patterns of group B samples prepared by microwave solid-state method with different SiC weight percentages: **a** 2θ range 20°–70° and **b** 2θ range 44°–46°

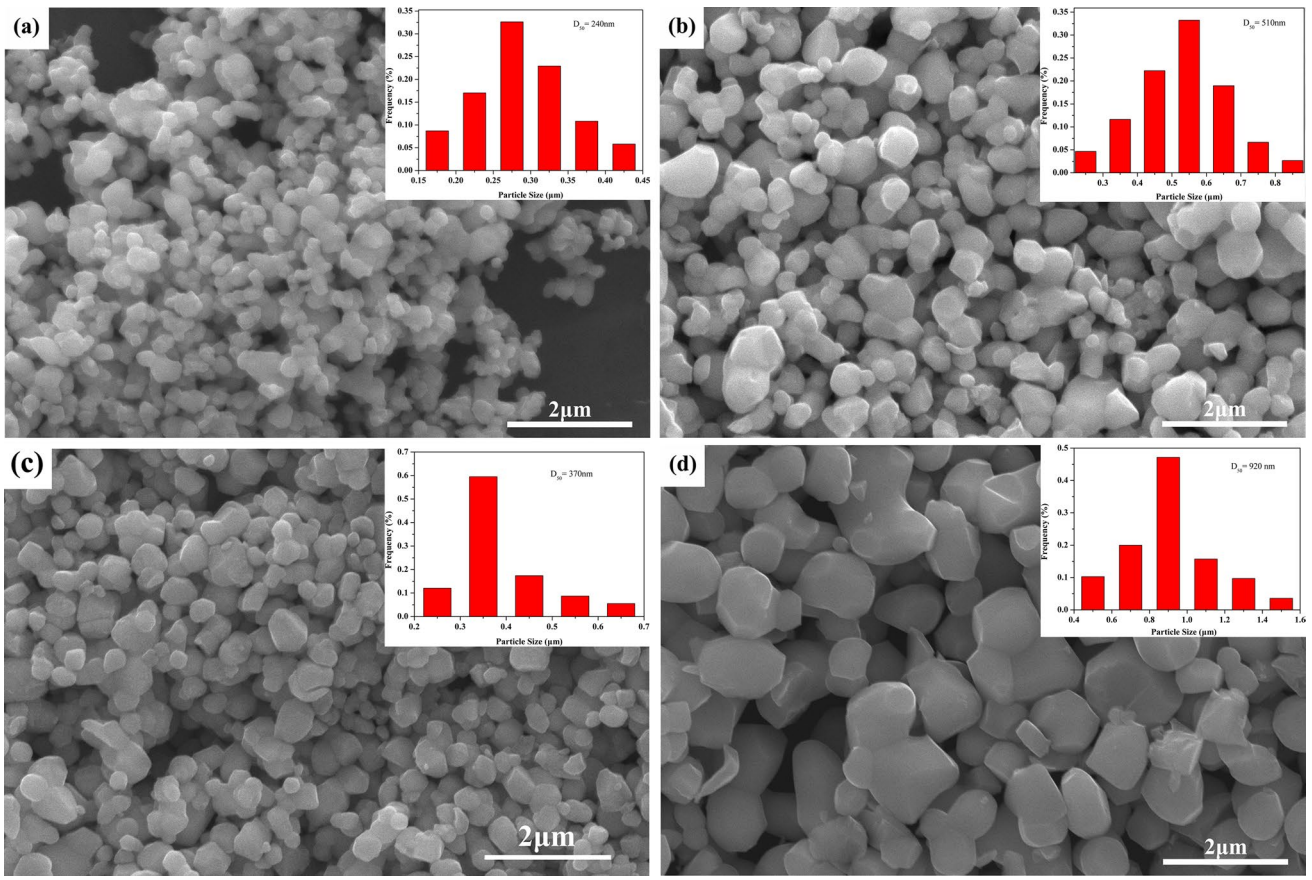

Fig. 7 SEM images of $BaTiO_3$ samples prepared by microwave solid-state method with different SiC contents: **a** 0 wt%, **b** 10 wt%, **c** 20 wt%, and **d** 25 wt%

was prepared without SiC, is severely agglomerated, with an average particle size of 240 nm. The particle size of the $BaTiO_3$ powder prepared with 10 wt% SiC is not uniform. The particle size varies from 300 to 600 nm, and the average size is 510 nm. These results show that the SiC was not

Table 4 Impurity elements in $BaTiO_3$ samples

Sample	Teat item and content (%)				
	Ba/Ti	SiO_2	CaO	SrO	MgO
S5	1.005	0.017	0.030	0.0034	0.0005
S6	1.007	0.014	0.037	0.0037	0.0007
S7	1.005	0.010	0.014	0.0030	0.0004
S8	1.006	0.012	0.029	0.0034	0.0008

Table 5 Statistical distributions of particle sizes

Sample	D_{10} (nm)	D_{50} (nm)	D_{90} (nm)	BET (m^2/g)
S5	170	240	400	8.13
S6	320	510	780	3.64
S7	280	370	540	7.32
S8	530	920	1250	1.87

well mixed with the raw materials and thermal runaway during heating led to abnormal grain growth. Figure 7c shows that the powder particles prepared with 20 wt% SiC are rectangular with good dispersibility and an average size of 370 nm. Unlike traditional solid-state methods, microwave irradiation gives a rapid temperature rise and uniform heating. This leads to rapid crystal nucleation and shortens the crystallization time. When SiC as a secondary acceptor is mixed with the powder, a micro-region heat source center is formed under the action of the microwave field, and uniform, rapid heating of the powder is achieved. The impurity content in sample S7 was determined by ICP-AES; the results are shown in Table 4. The results show a Ba/Ti ratio of 1.005:1 and no SiC impurities. Comparisons with the compositions of the raw materials shows that the impurities CaO, SrO, and MgO are derived from $BaCO_3$ and TiO_2, and the impurity SiO_2 is derived from SiC. The prepared samples meet the MLCC manufacturing requirements that are stipulated in the MLCC production manual. Figure 7d shows a SEM image of the sample prepared with 25 wt% SiC. The image shows that the average particle size of the sample is about 920 nm. The statistical distributions of the sample particle sizes are shown in Table 5; D_{10}, D_{50}, and D_{90} are the particle sizes corresponding to cumulative particle size distributions of 10%, 50%, and 90%, respectively. The specific surface areas were 8.13, 3.64, 7.32, and 1.87 m^2/g for the samples prepared with SiC contents of 0, 10, 20, and 25 wt%, respectively. The average particle size of $BaTiO_3$ increased with increasing SiC content. This is ascribed to the effect of the SiC content on microwave absorption. When the SiC content is low, the raw materials are not uniformly heated, and particle agglomeration is severe. When the SiC content is increased, thermal runaway occurs, and the average particle size is around 1 μm. This shows that if the SiC content is too high, side effects occur.

4 Conclusions

A $BaTiO_3$ powder of high tetragonality, with $c/a = 1.0085$, Ba/Ti = 1.005, and an average particle size of 370 nm was synthesized by microwave micro-region sintering at 850 °C for 2 h. Alanine facilitated the decomposition of $BaCO_3$ and improved the nucleation density of $BaTiO_3$. SiC effectively improved the uniformity of the synthesis temperature and enabled preparation of tetragonal-phase $BaTiO_3$ at low temperatures. This improved microwave solid-state method produces tetragonal $BaTiO_3$.

Acknowledgements We thank the Science and Technology Major Project of Guangxi (AA18118001), Guangxi Key Laboratory of Information Materials Foundation (No. 171021-Z).

References

1. X. Luo, S. Yuan, X. Pan, C. Zhang, S. Du, Y. Liu, ACS Appl. Mater. Inter. (2017). https://doi.org/10.1021/acsami.7b02580
2. Y. Wang, K. Miao, W. Wang, Y. Qin, J. Eur. Ceram. Soc. (2017). https://doi.org/10.1016/j.jeurceramsoc.2017.01.035
3. N. Liu, W. Zhao, J. Rong, J. Am. Ceram. Soc. (2018). https://doi.org/10.1111/jace.15339
4. J. Li, K. Inukai, Y. Takahashi, A. Tsuruta, W. Shin, J. Asian Ceram. Soc. (2018). https://doi.org/10.1016/j.jascer.2017.05.001
5. P. Xue, Y. Hu, W. Xia, H. Wu, X. Zhu, J. Alloys Compd. (2017). https://doi.org/10.1016/j.jascer.2017.05.001
6. J. Li, K. Inukai, Y. Takahashi, A. Tsuruta, W. Shin, Materials (2018). https://doi.org/10.3390/ma11050712
7. Z. Zhu, W. Zhu, Curr. Appl. Phys. (2018). https://doi.org/10.1016/j.cap.2018.04.016886-892
8. R. Ashiri, RSC Adv. (2016). https://doi.org/10.1039/c5ra22942a
9. S.-S. Ryu, D.-H. Yoon, J. Mater. Sci. (2007). https://doi.org/10.1007/s10853-007-1537-6
10. Y.A. Huang, B. Lu, D.D. Li, Z.H. Tang, Y.B. Yao, T. Tao, B. Liang, S.G. Lu, Ceram Int. (2017). https://doi.org/10.1016/j.ceramint.2017.09.027
11. J. Li, K. He, Z.-H. Zhou, H. Huang, L. Zhang, C.-G. Lou, H.-Y. Yu, Ceram. Int. (2017). https://doi.org/10.1016/j.ceramint.2017.07.229
12. H. Jiao, K. Zhao, R. Shi, L. Ma, Y. Tang, Cryst. Res. Technol. (2018). https://doi.org/10.1002/crat.201700107
13. A.Z. Simões, F. Moura, T.B. Onofre, M.A. Ramirez, J.A. Varela, E. Longo, J. Alloys Compd. (2010). https://doi.org/10.1016/j.jallcom.2010.08.143
14. K. Hongo, S. Kurata, A. Jomphoak, M. Inada, K. Hayashi, R. Maezono, Inorg. Chem. (2018). https://doi.org/10.1021/acs.inorgchem.8b00381
15. S. Ahda, S. Misfadhila, P. Parikin, T.Y.S.P. Putra, IOP Conf. Ser. Mater. Sci. Eng. (2017). https://doi.org/10.1088/1757-899x/176/1/012048

16. S.-S. Ryu, J. Kore. Powd. Met. Inst. (2012). https://doi.org/10.4150/kpmi.2012.19.4.310
17. C. Ando, H. Kishi, H. Oguchi, M. Senna, J. Am. Ceram. Soc. (2006). https://doi.org/10.1111/j.1551-2916.2006.00917.x
18. R. Yanagawa, M. Senna, C. Ando, H. Chazono, H. Kishi, J. Am. Ceram. Soc. (2007). https://doi.org/10.1111/j.1551-2916.2007.01498.x
19. O.G. Gromov, A.P. Kuzmin, G.B. Kunshina, R.M. Usmanov, E.P. Lokshin, Russ. J. Appl. Chem. (2008). https://doi.org/10.1134/s1070427208110025
20. R. Rotaru, C. Peptu, P. Samoila, V. Harabagiu, J. Am. Ceram. Soc. (2017). https://doi.org/10.1111/jace.15003
21. H. Itasaka, K.I. Mimura, K. Kato, Nanomaterials (2018). https://doi.org/10.3390/nano8090739
22. M. Bi, Y. Hao, J. Zhang, M. Lei, K. Bi, Nanoscale (2017). https://doi.org/10.1039/c7nr05212j
23. T.-T. Lee, C.-Y. Huang, C.-Y. Chang, I.K. Cheng, C.-L. Hu, C.-Y. Su, C.-T. Lee, M. Fujimoto, Int. Appl. Ceram. Technol. (2013). https://doi.org/10.1111/ijac.12072
24. T.M. Khan, M. Zakria, R.I. Shakoor, S. Hussain, Appl. Phys. A (2016). https://doi.org/10.1007/s00339-016-9766-7
25. L. Zhang, J.X. Wen, Z.X. Zhang, J. Yang, H. Huang, Q.Y. Hu, H.R. Zhuang, H.Y. Yu, Phys. B (2019). https://doi.org/10.1016/j.physb.2019.02.002
26. Y. Zhang, L. Wang, D. Xue, Powder Technol. (2012). https://doi.org/10.1016/j.powtec.2011.11.043
27. H.-W. Lee, S. Moon, C.-H. Choi, D.K. Kim, S.J. Kang, J. Am. Ceram. Soc. (2012). https://doi.org/10.1111/j.1551-2916.2012.05085.x
28. K. Tsuzuku, M. Couzi, J. Mater. Sci. (2012). https://doi.org/10.1007/s10853-012-6310-9
29. J.C. Niepce, G. Thomas, Solid State Ionics. (1990). https://doi.org/10.1016/0167-2738(90)90472-4
30. M.T. Buscaglia, M. Bassoli, V. Buscaglia, R. Alessio, J. Am. Ceram. Soc. (2005). https://doi.org/10.1111/j.1551-2916.2005.00451.x
31. C. Ando, H. Chazono, H. Kishi, Key Eng. Mater. (2004). https://doi.org/10.4028/www.scientific.net/KEM.269.161
32. C. Ando, K. Tsuzuku, T. Kobayashi, H. Kishi, S. Kuroda, M. Senna, J. Mater. Sci. Mater. Electron. (2008). https://doi.org/10.1007/s10854-008-9804-0